Uniport Journal of Engineering and Scientific Research (UJESR)

Vol. 9, Special Issue, 2024, Page 44-59
ISSN: 2616-1192

(www.ujesr.org)

Novel Sphericity-Dependent Drag Model for Accelerated Motion of Non-Spherical Particles in Viscous Medium

Big-Alabo Akuro[1]*, [1]Goodness Ofure Odah, [1]Millicent Obusor Osoh, [2]Celestine Ebieto Ebieto, [2]Joseph Chukwuka Ofodu and [1]Chinwuba Victor Ossia

[1]Applied Mechanics & Design (AMD) Research Group, Department of Mechanical Engineering, Faculty of Engineering, University of Port Harcourt, Port Harcourt, Nigeria

[2]Energy and Thermofluid Engineering (ETE) Research Group, Department of Mechanical Engineering, Faculty of Engineering, University of Port Harcourt, Port Harcourt, Nigeria

*Correspondence Email: *akuro.big-alabo@uniport.edu.ng*

Abstract

A novel sphericity-dependent drag model for the accelerated motion of non-spherical particles in Newtonian fluids has been developed. The main advantage of the model is that it has a simple Reynolds number dependence that is suitable for analytical solutions of accelerated particle motion. The present model was developed using nonlinear regression analysis of simulated data obtained from a published model with complex Reynolds number dependence. The present model was validated with published experimental data having sphericities of 0.471 – 1.00 and valid for Reynolds number of 0.01 – 10000. An error analysis of the present model and other published sphericity-dependent models showed that the present model had the lowest root-mean-square error. Therefore, the present drag model was applied to derive closed-form solutions for the accelerated motion of a non-spherical particle and a new settling velocity formula. The closed-form solutions were used to investigate the effect of sphericity on the accelerated motion for non-zero initial velocity.

Keywords: *Coefficient of drag, Sphericity, Non-spherical particle, Nonlinear regression, Accelerated motion of particle fall, Settling velocity*

Received: 14th December, 2024 *Accepted: 31st December, 2024*

1. Introduction

Understanding the motion of a rigid particle falling in a fluid medium is significant for both scientific and engineering endeavors with far-reaching applications spanning from sedimentation processes (Julien, 2010), hydraulics laboratories (Guo, 2011), microfluidic systems (Krafcik et al., 2018), powder technology (Jalaal et al., 2010a), bubble transport (Allen, 1900; Chen et al., 2022), drilling operations (Chien, 1994), multiphase flow (Bombardelli and Chanson, 2009), microphysics of clouds (Crowe et al., 2011), volcanology (Dioguardi et al., 2018) and combustion processes (Big-Alabo and Ezekwem, 2021) to the formation of marine aggregates (Maggi, 2013) and disease control (Liu et al., 2022). Laminar particle flows occur at very low Reynolds numbers and are characterized by a distinctive drag law. This law, known as the Stokes drag law, was initially proposed by George Gabriel Stokes (1819–1903) as a first approximation of the Navier-Stokes equation. In contrast, turbulent particle flow is characterized by a Reynolds number that is much greater than unity and exhibits significant flow separation from the particle surface. The turbulent regime, known as Newton flow, has a drag coefficient that is generally independent of the Reynolds number. Analytical solutions for particle motion in Stokes and Newton flows are readily derivable. The challenge arises in the transitional flow regime, where the drag force has a strong nonlinear dependence on the Reynolds number. At the moment, there is no known exact theoretical solution for the drag law of the transitional regime. In practice, the transitional flow models are obtained by analytical approximations or empirical correlations.

Many empirical drag laws have been developed for spherical particles in transitional flow. Goossens (2019) reviewed drag models for the transitional regime of a spherical particle motion. He conducted a comparative analysis of various spherical drag models and concluded that the

Rubey's drag model stands out for its simplicity and accuracy. In Rubey's model, the drag coefficient is partially constant and partially inversely proportional to the Reynolds number as shown in Equation (1).

$$C_d = \frac{A}{Re} + B \tag{1}$$

where C_d is the drag coefficient, and A and B are fitting parameters. Guo (2011) suggested typical values of the fitting parameters for spherical particles as: $A = 24$ and $B = 0.44 \pm 0.06$ i.e. B ranges from 0.38 – 0.50. He used $B = 0.39$ in his theoretical solution to predict the experimental data of Moorman (1955) accurately. Yin et al. (2017) proposed $A = 25.057$ and $B = 0.5$, Loth (2008) used $A = 24$ and $B = 0.4$, whereas Goossens (2019) recommends $A = 24$ and $B = 0.44$ for spherical particles. Equation (1) does not introduce any additional nonlinearity in the differential equation for accelerated motion neither does it introduce any complexities in the existing nonlinearities (Lain et al., 2023). Hence, Equation (1) has been used in several studies to derive analytical solutions for the accelerated motion of a spherical particle (Ferreira et al., 1998; Jalaal et al., 2010a; Guo, 2011; Torabi and Yaghoobi, 2012; Yin et al., 2017).

In most practical cases, the gravitational fall of a particle in a viscous medium involves non-spherical particles. In contrast to the drag coefficient for spherical particles that depends on the Reynolds number only, the drag coefficient for non-spherical particles depends on the shape of the particle in the fall direction and the Reynolds numbers. Several shape factors and parameters have been proposed to account for the effect of particle shape and orientation on the drag coefficient of non-spherical particles (see for example the review by Michaelides and Feng (2023)). However, the most common shape factor used to account for the shape of non-spherical particles is the sphericity (ϕ). It was first introduced by Wadell (1934) and it is defined as the ratio of the surface area of a sphere having the same volume as the particle (A_s) to the actual area of the particle (A_p) i.e. $\phi = A_s/A_p$. The sphericities of regularly-shaped non-spherical particles can be determined precisely (Li et al., 2012) but the sphericities of irregularly-shaped particles are determined using approximate methods (Liu et al., 2022).

Haider and Levenspiel (1989) demonstrated that a drag law for spherical particles could be applied to non-spherical particles if the fitting parameters are recalibrated for each sphericity. They derived correlations between the four fitting parameters and sphericity using 506 data points consisting of 419 data points for isometric particles and 87 data points for disc particles. They applied the correlated results to formulate a sphericity-dependent drag law for non-spherical particles as shown:

$$C_d = \frac{24}{Re}\left[1 + \exp(2.3288 - 6.4581\phi + 2.4486\phi^2)\, Re^{(0.0964 + 0.5565\phi)}\right] + \frac{Re \times \exp(4.905 - 13.8944\phi + 18.4222\phi^2 - 10.2599\phi^3)}{Re + \exp(1.4681 + 12.2584\phi - 20.7322\phi^2 + 15.8855\phi^3)} \tag{2}$$

Equation (2) is applicable to sphericities in the range of 0.026 – 1.00 and for $Re < 25000$. A drawback of Equation (2) is that it is too complex for theoretical analysis of accelerated motion and it does not reduce to the drag law for spherical particles from which it was derived when $\phi = 1.0$.

Chien (1994) developed a drag law for irregular particles settling in both Newtonian and non-Newtonian fluids. The drag law was developed by correlating a data set from drill cuttings in reservoir fluids and natural minerals in high viscosity fluids. Michaelides and Feng (2023) recommended that the drag law of Chien (1994) should be applied to particle fall in high viscosity fluids whereas Big-Alabo et al. (2023) showed that the drag law of Chien (1994) accurately predicts the drag curves of isometric particles having sphericities of 0.67 – 1.00. The drag model of Chien (1994) is given as:

$$C_d = \frac{30}{Re} + \frac{67.287}{e^{5.03\phi}} \tag{3}$$

Equation (3) has the same form as Equation (1), the only difference being that the constant B in Equation (1) is now replaced by a function of sphericity in Equation (3). One limitation of Equation (3) is that it cannot be reduced to the Stokes drag law when $\phi = 1.0$ and $Re < 1$. However, it has the advantage that it does not introduce additional or complex nonlinearities in the differential equation of the accelerated motion (Lain et al., 2023). Consequently, it has been an ideal candidate for analytical investigations on the accelerated motion of non-spherical particles (Jalaal

et al., 2010b; Yaghoobi and Torabi, 2012; Zolfagharian et al., 2017; Big-Alabo et al., 2023; Lain et al., 2023).

Yow et al. (2005) used a three-parameter empirical drag correlation for spherical particles to develop a sphericity-dependent drag law for non-spherical particles. The drag law accounts for sphericities in the range of 0.006 – 1.00 and Reynolds number in the range of 0.01 – 100000. The drag law of Yow et al. (2005) is given as:

$$C_d = \frac{\left(15.21 + \frac{10.82}{\phi} - \frac{0.14}{\phi^2}\right)}{Re} + \frac{\left(13.14 - \frac{10.64}{\phi} - \frac{0.06}{\phi^2}\right)}{\sqrt{Re}} - 8.82 + \frac{5.70}{\phi} + \frac{0.23}{\phi^2} \quad (4)$$

Although Equation (4) appears to be relatively simple compared to most of the other sphericity-dependent drag laws, it does not reduce to the Stokes' drag law when $\phi = 1.0$ and $Re < 1$. Also, the application of Equation (4) to the differential equation of the accelerated motion will introduce fractional nonlinearity which is difficult to solve analytically.

Dioguardi et al. (2018) also applied the four parameter drag law for spherical particles proposed by Haider and Levenspiel (1989) to develop a sphericity-dependent drag law for non-spherical particles with Reynolds number in the range of 0.03 – 10000. They expressed the four parameter drag law for spherical particles as the sum of three components representing the Stokes, transitional and Newton flow regimes respectively. Then, they introduced sphericity-based functions for each component and derived the unknown constants in the functions based on two constraints and minimization of the error in predicting measured settling velocities. The first constraint requires that the sphericity-based functions must all evaluate to unity when $\phi = 1.0$, while the second constraint requires that the ratio of the component drag coefficient to the total drag coefficient for a sphere should be equal to the corresponding ratio for the measured data. The experimental data used consisted of 304 terminal velocity measurements carried out on 143 volcanic ash and lapilli particles. The drag model of Dioguardi et al. (2018) is given as:

$$C_d = \frac{24}{Re}\left(\frac{1-\Psi}{Re} + 1\right)^{0.25} + \frac{24}{Re}(1 + 0.1806Re^{0.6459})\Psi^{-Re^{0.08}} + \left(\frac{0.4251}{1 + 6880.95/Re}\right)\Psi^{5.05} \quad (5)$$

where $\Psi = \phi/X$ is a shape factor defined as the ratio of the sphericity (ϕ) to the circularity (X). Due to the application of the first constraint, Equation (5) reduces to the drag law for a spherical particle when $\phi = 1.0$. Therefore, the limitation of Equation (2) was resolved in Equation (5). Yang et al. (2021) applied the approach of Dioguardi et al. (2018) to derive a sphericity-dependent drag law for non-spherical particles with sphericities of 0.421 – 1.0 and Reynolds number in the range of 0.008 – 10000. Their model is based on the spherical drag law of Clift and Gauvin (1971) and the sphericity-based functions were correlated using 828 experimental data points obtained from the literature. The drag law of Yang et al. (2021) is given by:

$$C_d = \frac{24}{Re}(2-\phi)^{1.29} + \frac{24}{Re}(1 + 0.15Re^{0.687})\phi^{-Re^{0.134}} + \left(\frac{0.42}{1 + 42500/Re^{1.16}}\right)e^{1.43(1-\phi)} \quad (6)$$

Yang et al. (2021) examined the accuracy of their drag law with those of Dioguardi et al. (2018), Chien (1994) and three others. The drag law of Yang et al. (2021) produced the least relative error and the least root-mean-square error when compared to the measured data of settling velocity. Hence, Equation (6) was used in this study to simulate data with which the sphericity-based functions of the present drag law were correlated.

Other sphericity-dependent drag laws for non-spherical particles have been proposed and are discussed extensively in the review article by Michaelides and Feng (2023). Some of these drag laws account for particle fall orientation and other shape characterization parameters apart from the sphericity (Bagheri and Bonadonna, 2016). The drag laws derived based on orientation and other shape parameters, and almost all the sphericity-dependent drag laws are not suitable for analytical studies of the accelerated particle motion due to their complicated nonlinear dependence on Reynolds number. An exception is the drag law of

Chien (1994), which has a simple Reynolds number dependence as the Rubey's drag law. However, the drag law of Chien (1994) has several shortcomings. First, it does not give an accurate prediction of Stokes flow for spherical particles (Goossens, 2019). Secondly, it produces large deviations from experiments for sphericities less than 0.67 (Big-Alabo et al., 2023). Thirdly, it does not capture the variation in the slope of the Stokes flow for non-spherical particles as observed from experiments (see Figure 1 in Haider and Levenspiel (1989) and Figure 1 in Big-Alabo et al. (2023)). The reason is that the data used in correlating the drag law of Chien (1994) does not show any significant variation in the Stokes regime. However, other studies (Haider and Levenspiel, 1989; Big-Alabo et al., 2023) have shown that such variation exists. In order to address these shortcomings a novel sphericity-dependent drag law was derived in the present study. The present drag law has the same Reynolds number dependence as in Equation (1) but the fitting parameters A and B are both replaced by sphericity-based functions that were correlated using nonlinear regression analysis. The present drag law was validated using published experimental data on the $C_d - Re$ relationship for sphericities in the range of 0.471 – 1.00 and Reynolds number in the range of 0.01 – 10000. Application of the present drag law to derive analytical solutions for the unsteady (i.e. accelerated) and steady motions of a non-spherical particle was also discussed.

2. Formulation of new sphericity-based drag law

The motivation for this study is the formulation of a sphericity-dependent drag law for theoretical analysis of non-spherical particles that has the same $C_d - Re$ relationship as the Rubey's drag law. To achieve this, the parameters A and B in Equation (1), which represent fitting parameters for the Stokes and Newton flows respectively (Goossen, 2019), are assumed to depend on the sphericity. This assumption is justified in view of the fact that previous studies have provided sphericity-based corrections to the Stokes and Newton regimes for non-spherical particles (Ganser, 1993; Dioguardi et al., 2018; Yang et al., 2021). In order to determine the effect of sphericity on the values of A and B, we used the drag law of Yang et al. (2021) to simulate 29,990 data points for each sphericity considered and for Reynolds number in the range of $0.1 - 200000$. The simulated data from the drag model of Yang et al. (2021) was used for correlation because the published experimental data for each sphericity are insufficient to provide a good fit for simple models like Equation (1).

The present approach is perfectly okay because the goal is to extract a simple model of similar accuracy as the complicated but accurate model of Yang et al. (2021). Yin et al. (2017) applied the same approach to obtain the constants in Equation (1) for spherical drag in transitional flow using simulated data from the more complicated drag model of Lapple and Shepherd (1940). Since the drag law of Yang et al. (2021) was derived for sphericities of 0.421 – 1.0, the range of sphericities considered in the simulations is 0.45 – 1.0. The simulated data were exported into Mathematica software package where a nonlinear regression analysis was conducted using the "NonlinearModelFit" function to find the best values for A and B for each sphericity. The results of the regression analysis are summarized in Table 1 and the correlation coefficients (R^2-values) confirm that very good fits were obtained. The results of the root-mean-square error (RMSE) show that the deviation of Equation (1) from the drag law of Yang et al. (2021) is not significant. Table 1 also confirms that the slope of the Stokes regime increases gradually as the sphericity decreases.

The next step in deriving the present drag law is to choose two sphericity-based functions (i.e. $A(\phi)$ and $B(\phi)$) that can correlate the results in Table 1. To ensure that the functions satisfy well-established drag theory, observations from experimental data, and provide a good correlation of the data in Table 1, certain constraints were considered in choosing the functions. For the first function, it is required that $A(\phi = 1) = 24.0$ in order to satisfy Stokes drag law. Additionally, $A(\phi_{j+1}) > A(\phi_j) > 24.0$ for $\phi_{j+1} < \phi_j < 1.0$ in order to capture the variation of the drag curve with sphericity as observed from experimental data (Haider and Levenspiel, 1989; Big-Alabo et al., 2023). Chien (1994) used $A(\phi) = 30.0$ which satisfies neither the Stokes drag law for $\phi = 1$ nor the observed variation of the drag curve with sphericity. For the second function, the constraint $B(\phi_{j+1}) > B(\phi_j)$ for $\phi_{j+1} < \phi_j < 1.0$ was applied to capture the observed variation of the drag curve with sphericity. Based on the above constraints, the following sphericity-based functions were chosen to fit the data in Table 1.

$$A(\phi) = 24(2 - \phi)^{\alpha} \quad (7a)$$

$$B(\phi) = (\Gamma - 0.44)e^{-\beta\phi} + 0.44 \quad (7b)$$

Table 1: Best fit values of A and B for various sphericities

ϕ	A	B	R^2	RMSE
0.450	43.5701	4.35886	0.975762	0.873163516
0.475	42.8913	3.62206	0.985764	0.591939903
0.500	42.4418	3.05785	0.991542	0.412761914
0.525	41.3459	2.61811	0.994514	0.305974984
0.550	40.5196	2.26981	0.995794	0.249942063
0.575	39.6738	1.98981	0.996147	0.225423434
0.600	38.8160	1.76164	0.996049	0.216724768
0.625	37.9515	1.57336	0.995772	0.214058225
0.650	37.0838	1.41617	0.995457	0.212724473
0.675	36.2157	1.28353	0.995172	0.210914044
0.700	35.3488	1.17049	0.994939	0.20813403
0.725	34.4847	1.07326	0.994763	0.204412582
0.750	33.6243	0.988921	0.994638	0.199948366
0.775	32.7682	0.915182	0.994554	0.194967745
0.800	31.9171	0.850242	0.994500	0.189672294
0.825	31.0713	0.792665	0.994468	0.184224096
0.850	30.2311	0.741298	0.994450	0.178746019
0.875	29.3967	0.695207	0.994438	0.173327197
0.900	28.5684	0.65363	0.994429	0.168029662
0.925	27.7463	0.615942	0.994418	0.162894517
0.950	26.9304	0.581624	0.994401	0.157947149
0.975	26.1209	0.550244	0.994377	0.153201409
1.000	25.3179	0.521441	0.994343	0.148662861

where α, β and Γ are fitting parameter. Equation (7a) is the same as the function used by Yang et al. (2021) for the Stokes regime while Equation (7b) is an exponential function that attempts to account for the logarithmic variation of the $C_d - Re$ relationship in the transitional and Newton regimes. Again, the NonlinearModelFit function in Mathematica was used to fit Equations (7a) and (7b) to the data in Table 1 and the best fit values obtained for α, β and Γ were 1.42229, 6.79646 and 80.8527 respectively. Figure 1 compares the data in Table 1 with simulations of Equations (7a) and (7b) using the correlated values obtained for α, β and Γ. The plots show a good agreement between the data in Table 1 and the predictions of Equations (7a) and (7b). This is not surprising considering that the R^2-values obtained from fitting Equations (7a) and (7b) to the data in Table 1 were 0.99947 and 0.999036 respectively. Therefore, the correlated sphericity-based functions are:

$$A(\phi) = 24(2-\phi)^{1.42229} \quad (8a)$$

$$B(\phi) = 80.4127e^{-6.79646\phi} + 0.44 \quad (8b)$$

Substituting Equations (8a) and (8b) in (1) gives the new sphericity-dependent drag law as:

$$C_d = \frac{24(2-\phi)^{1.42229}}{Re} + 80.4127e^{-6.79646\phi} + 0.44 \quad (9)$$

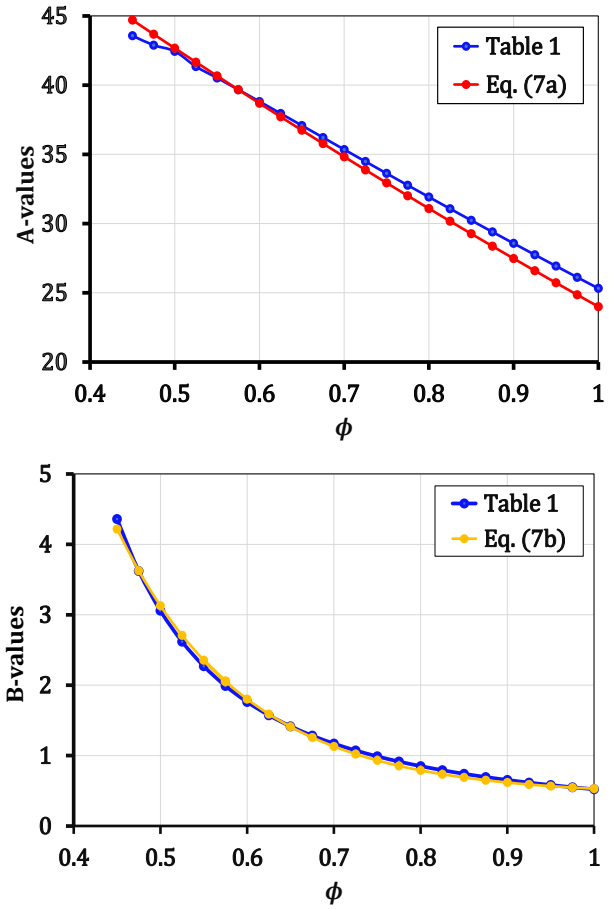

Fig. 1: Comparison of Table 1 data and estimates of Equations (7)

Equation (9) has the same Reynolds number dependence as the Rubey's drag model and can be used to obtain analytical solutions of the accelerated motion of a non-spherical particle. Before carrying out such investigation, it is necessary to validate Equation (9) with experimental data and results of published sphericity-dependent drag laws. This validation was presented in Section 3.

3. Experimental validation

In this section, the new sphericity-dependent drag law in Equation (9) was validated by comparing with experiments on non-spherical particles (Yang et al., 2021). The experimental data consist of 828 data points representing particles with sphericities of $0.421 \leq \phi \leq 1.0$ and covering flow regimes in the range $0.008 \leq Re \leq 10000$. In this experimental database, the sphericity of 0.421 has only one data point and is considered as an outlier. Therefore, the remaining 827 data points representing particles with sphericities of $0.471 \leq \phi \leq 1.0$ were used in the present validation. The present drag law was simulated using the ϕ-values and Re-values of the experimental data. The simulation was compared to the measured C_d values of the 827 data points and the maximum relative error (MARE), minimum relative error (MIRE) and RMSE were computed. Similar simulations and comparison with the measured C_d values were carried out using the drag laws of Haider and Levenspiel (1989), Chien (1994), and Yang et al. (2021). The results are summarized in Table 2.

The relative error (RE) and RMSE were respectively calculated as:

$$RE(\%) = \left|\frac{C_{d,pred} - C_{d,meas}}{C_{d,meas}}\right| \times 100\% \quad (10)$$

$$RMSE = \sqrt{\frac{1}{n}\sum_{j=1}^{n}\left(C_{d,pred} - C_{d,meas}\right)_j^2} \quad (11)$$

where $C_{d,pred}$ is the predicted drag coefficient using the drag laws, $C_{d,meas}$ is the measured drag coefficient and $n = 827$ is the number of data points. The maximum and minimum errors were determined as $MARE = Max\{RE_{j1}\}$ and $MIRE = Min\{RE_{j1}\}$ for $j = 1,2,3,\ldots,827$ where $\{RE_{j1}\}$ is a column vector of the relative errors of all data points. Table 2 shows that the present drag law has the least MIRE and RMSE values. Also, Equation (6) has the least MARE followed by the present drag law which is very close to Equation (6). The MARE and MIRE are not good measures of the error analysis because they only consider extreme results. On the other hand, the RMSE is a good measure of the error analysis because it accounts for all data points. From the error analysis, we can say that the present drag law appears to be as good as the drag law of Yang et al. (2021) although it is much simpler.

Table 2: Error analysis of present drag law in comparison with other sphericity-dependent drag laws

Model	MARE (%)	MIRE (%)	RMSE
Haider and Levenspiel (1989) – Equation (2)	192.2454388	0.059736006	92.69716717

Chien (1994) – Equation (3)	327.271235	0.039017185	78.67856526
Yang et al. (2021) – Equation (6)	149.3805632	0.020127240	68.71635843
Present drag law – Equation (9)	157.7303063	0.002924519	67.61610847

The validity of the present drag law was further examined by comparing its $C_d - Re$ plot with other drag laws and measured data. The other drag laws are those of Haider and Levenspiel (1989), Chien (1994), and Yang et al. (2021). The measured $C_d - Re$ data used in the comparison were obtained from Yang et al. (2021) for $\phi \leq 0.874$, Haider and Levenspiel (1989) for $\phi = 0.906$ and Lapple and Shepherd (1940) for $\phi = 1.000$. The $C_d - Re$ plots for various sphericities are shown in Figure 2. The plots reveal that the present drag law produced a similar prediction as Yang et al. (2021) and gives better prediction than Haider and Levenspiel (1989) and Chien (1994) for $\phi < 0.67$. For $\phi \geq 0.67$, the present drag law still performs very well and gives similar results to Yang et al. (2021) for $Re < 10$ and $Re > 500$. For the flow range of $10 \leq Re \leq 500$ in the transitional regime, the present drag law shows significant deviation from the drag law of Yang et al. (2021) when $\phi \geq 0.67$. This occurs because the present drag law is a direct combination of the observed drag behaviour in the Stokes and Newton regimes. A similar observation has been reported by Goossens (2019) concerning the Rubey's drag law for spherical particles. Nevertheless, the present drag law and the drag law of Yang et al. (2021) provided a more accurate prediction of the Stokes regime ($Re < 1.0$) in all cases. In conclusion, the present drag law provides a good estimate of the drag behaviour of non-spherical particles.

4. Settling velocity

The settling velocity is one of the key data for particulate analysis. It can be used for particle sizing (Guo, 2011), viscosity measurement, electrical charge measurement and to determine the coefficient of drag. Several formulas have been proposed to determine the settling velocity of spherical and non-spherical particles (Cheng, 2009; Haider and Levenspiel, 1989; Chien, 1994). Most of the settling velocity formulas are derived empirically and show an explicit relationship between the settling velocity and the nominal diameter of the particle. The relationship between the settling velocity and the properties of the fluid and particle are not known in these empirical formulas. Here we used the present drag law to derive a closed-form settling velocity formula for non-spherical particles that is dependent on the on the properties of the fluid and particle.

The settling velocity of a particle is attained at the onset of the steady motion during which all inertia forces are zero and the viscous force is equal to the apparent weight of the particle. Therefore, we can write the following equation for steady motion of a dense particle falling in a quiescent fluid medium:

$$\frac{1}{2}\rho_f C_d A_p u_s^2 - (\rho_p - \rho_f)V_p g = 0 \qquad (12)$$

where ρ_f is the density of the fluid, ρ_p is the density of the particle, $C_d = f(\phi, Re_s)$ is the drag coefficient at the setting velocity, u_s is the settling velocity, A_p is the projected area of the particle in the fall direction and g is the gravitational acceleration. The first term in Equation (12) is the drag force while the second term is the apparent weight. Substituting Equation (9) in (12), gives equation (13) as follows:

$$\frac{1}{2}\rho_f A_p u_s^2 \left(\frac{24(2-\phi)^{1.42229}}{Re_s}\right) + \frac{1}{2}\rho_f A_p u_s^2 \left(80.4127e^{-6.79646\phi} + 0.44\right) - (\rho_p - \rho_f)V_p g = 0 \qquad (13)$$

If the nominal diameter is D, then $A_p = \pi D^2/4$ and $V_p = \pi D^3/6$. Also, the Reynolds number at the settling velocity is $Re_s = u_s D/v$ where v is the kinematic viscosity of the fluid. Then,

$$au_s^2 + bu_s - c = 0 \qquad (14)$$

where $a = 40.20635e^{-6.79646\phi} + 0.22$, $b = 12(2-\phi)^{1.42229}v/D$ and $c = 2gD(\sigma - 1)/3$. Solving Equation (14) gives:

$$u_s = \frac{\sqrt{b^2 + 4ac} - b}{2a} \qquad (15)$$

from which the formula of the settling velocity was derived as Equation (16).

$$u_s = \frac{\sqrt{144v^2(2-\phi)^{2.84458} + 4gD^3(\sigma-1)(80.4127e^{-6.79646\phi} + 0.44)/3} - 12v(2-\phi)^{1.42229}}{(80.4127e^{-6.79646\phi} + 0.44)D} \qquad (16)$$

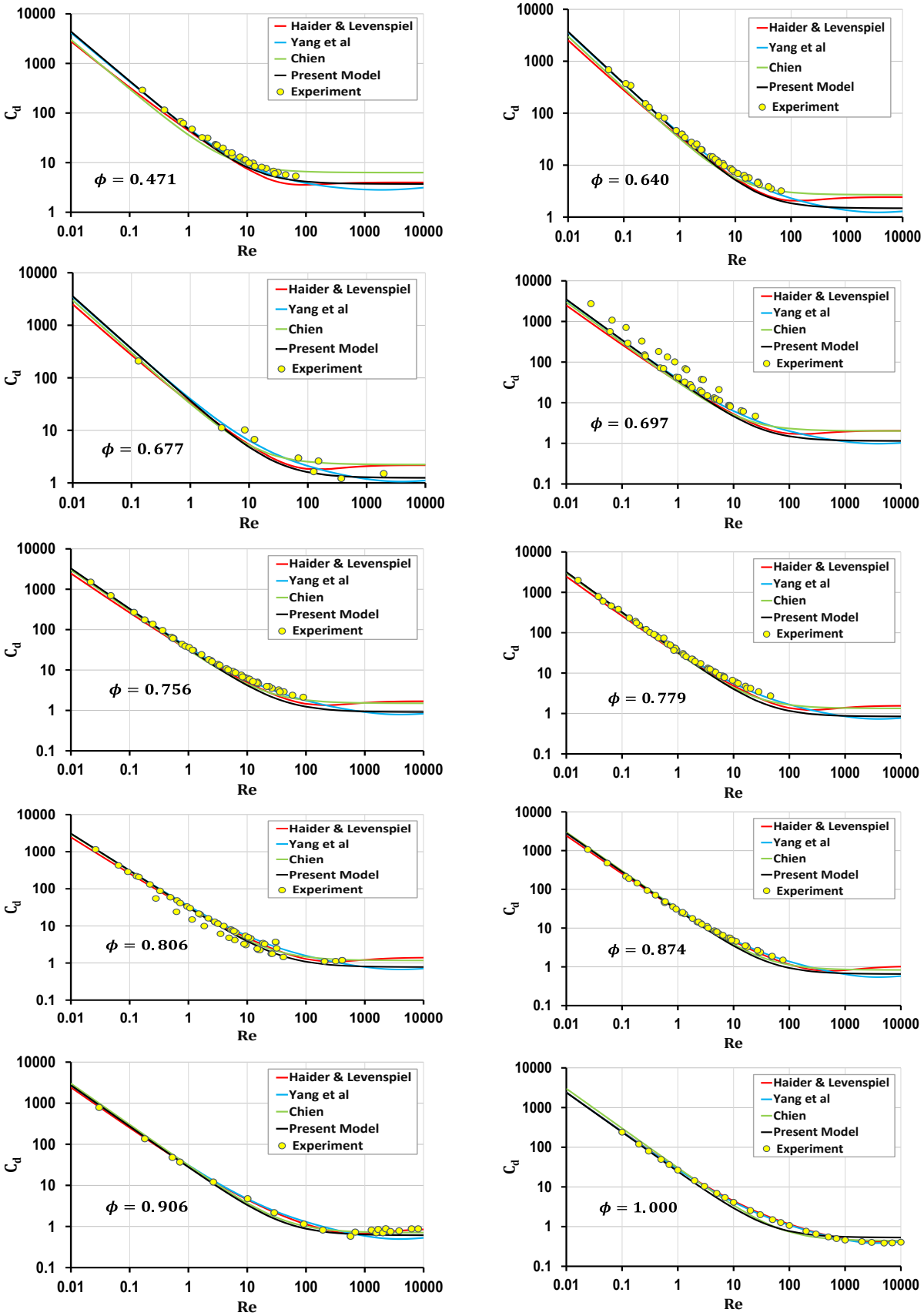

Fig. 2: $C_d - Re$ plots for various sphericities: comparison of drag laws with measured data

Equation (16) is a closed-form formula for calculating the theoretical settling velocity of non-spherical particles with sphericities in the range $0.471 \leq \phi \leq 1.0$ and for $Re_s < 10000$. The settling velocity is dependent on the sphericity of the particle and the material and geometric properties of the particle and fluid. Equation (16) can be written in non-dimensional form as follows:

$$\bar{u}_s = \frac{\sqrt{144(2-\phi)^{2.84458} + (80.4127e^{-6.79646\phi} + 0.44)\bar{D}^3} - 12(2-\phi)^{1.42229}}{80.4127e^{-6.79646\phi} + 0.44} \quad (17)$$

where $\bar{u}_s = u_s D/v$ and $\bar{D} = (\sigma - 1)(4g/3v^2)^{1/3} D$ are the non-dimensional settling velocity and diameter respectively. The non-dimensional settling velocity is also equal to the Reynolds number at the settling velocity. In reality, the theoretical settling velocity is never attained exactly but it is only approached asymptotically. For practical purposes the actual settling velocity is normally taken as $100(1 \pm 0.01)\%$ of the theoretical settling velocity (Guo, 2011; Yin et al., 2017; Big-Alabo et al., 2023). Therefore, when $u_0 < u_s$, $u_s^a = 0.99u_s$ at $t = t_s$ and when $u_0 > u_s$, $u_s^a = 1.01u_s$ at $t = t_s$, where u_s^a is the actual settling velocity of the particle.

Figures 3 and 4 show the predictions of Equation (16) compared with experiments (Hazzab and Terfous, 2008) of non-spherical PVC and glass particles falling in water and oil. The material properties of the particles and fluid are given in Table 3. The log-log plot of the settling velocity against the diameter is a straight line relationship (Terfous et al., 2013) and was applied in Figures 3 and 4. Equation (16) provides a good prediction of the experimental data especially for the more viscous oil medium. Figure 5 demonstrates the effect of sphericity on the settling velocity-diameter profile using normal, log-normal and log-log plots. The data used for the simulation are those of glass and water. The simulations show that a decrease in the sphericity results in a decrease in the settling velocity for any given diameter. This is due to the fact that a lower sphericity results in a higher drag force which causes the particle to settle faster. Hence, the settling velocity, settling distance and settling time all decrease with the sphericity.

Table 3: Properties of water, oil, PVC and glass

Property	Water	Oil	PVC	Glass
$\rho\ (kg/m^3)$	1000.0	793.0	1380.0	2640.0
$v\ (m^2/s)$	1.0×10^{-6}	2.19×10^{-3}	n/a	n/a

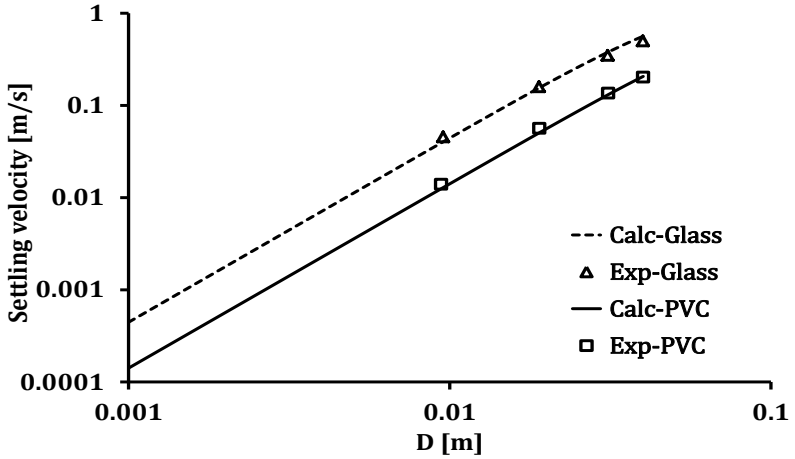

Fig. 3: Prediction of settling velocity of glass and PVC cylindrical particles in oil for $\phi = 0.804$. Lines – Equation (16); markers – measured data (Hazzab and Terfous, 2008).

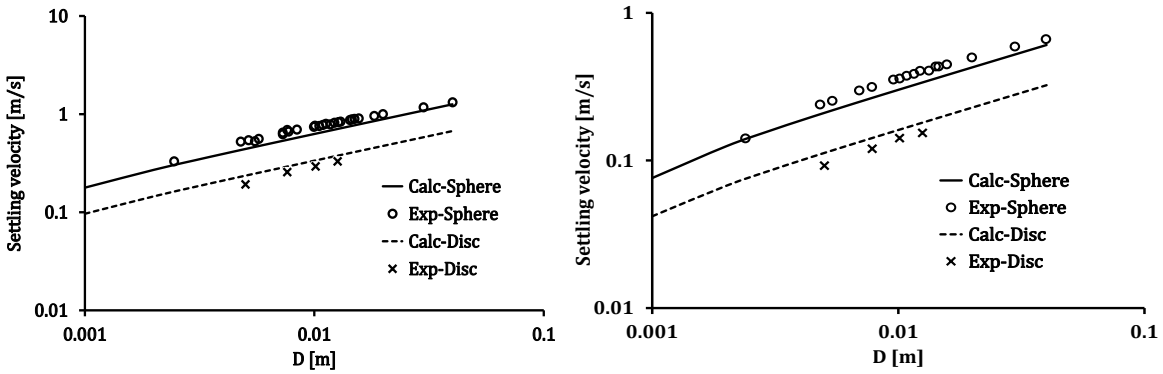

Fig. 4: Prediction of settling velocity of PVC (left plot) and glass (right plot) particles in water: sphere ($\phi = 1.0$) and disc ($\phi = 0.594$). Lines – Equation (16); markers – exp. data (Hazzab and Terfous, 2008)

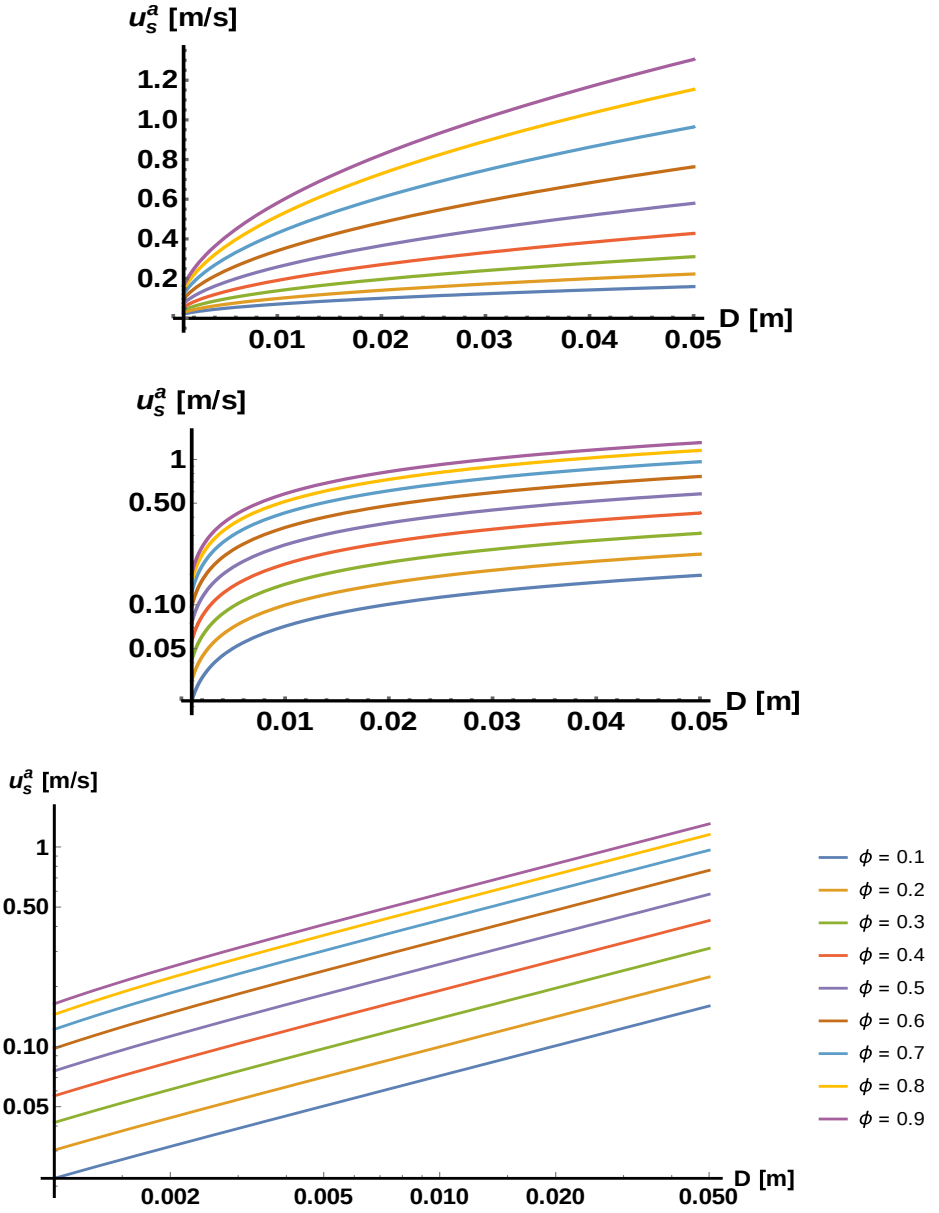

Fig. 5: Variation of settling velocity with sphericity. Normal (top left), Log-normal (top right) and Log-log (bottom centre) plots. The legend of the bottom plot is the same for the top plots.

5. Accelerated motion of non-spherical particles

The forces acting on a freely falling non-spherical particle in a still viscous fluid are shown in Figure 6 and the balance of forces is given as:

$$m_p \frac{du}{dt} = W_p - W_{df} - F_d - F_{AM} - F_{Ba} \qquad (18)$$

where $u = ds/dt$ is the particle velocity, W_p is the weight of the particle, W_{df} is the weight of the displaced fluid which is equal to the upthrust or buoyancy force, F_d is the drag force, F_{AM} is the added mass force, F_{Ba} is the Basset history force and m_p is the mass of the particle. The terms on the right hand side of Equation (18) are:

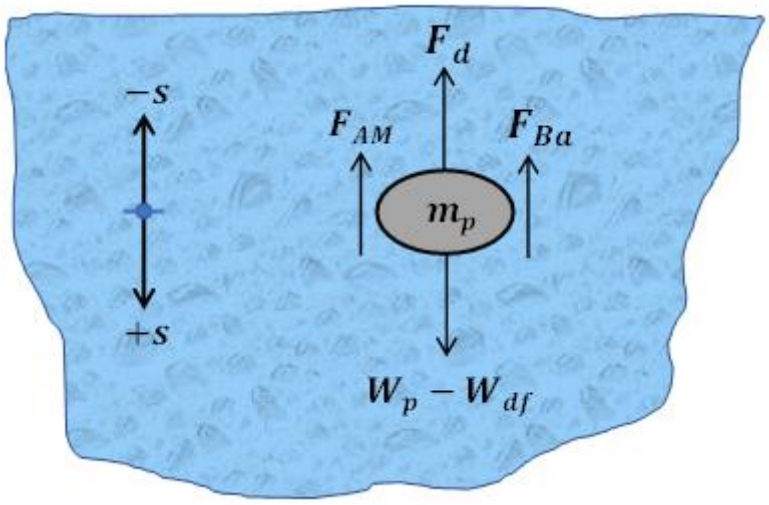

Fig. 6: Balance of forces during gravitational fall of a rigid non-spherical particle in a viscous fluid (adapted from Big-Alabo and Ofodu, 2024)

$$W_p - W_{df} = (\rho_p - \rho_f)V_p g = \frac{\pi}{6}D^3(\rho_p - \rho_f)g \qquad (19a)$$

$$F_D = \frac{1}{2}C_d\rho_f A_p u^2 = \frac{\pi}{8}C_d\rho_f D^2 u^2 \qquad (19b)$$

$$F_{AM} = C_a m_f \frac{du}{dt} = \frac{\pi}{6}C_a D^3 \rho_f \frac{du}{dt} \qquad (19c)$$

$$F_{Ba} = \frac{3}{2}D^2\sqrt{\pi\rho_f \nu}\int_0^t \frac{du}{d\tau}\frac{d\tau}{(t-\tau)^{1/2}} \qquad (19d)$$

where ρ_p is the density of the particle, ρ_f is the density of the fluid, V_p is the volume of the particle, g is gravitational acceleration, D is the diameter of the volume equivalent sphere, C_a is the added mass coefficient, m_f is the mass of displaced fluid and τ is a dummy integration variable. Substituting Equations (19a-d) into (18) gives the classical Boussinesq-Basset-Oseen (BBO) equation as follows:

$$\frac{\pi}{6}D^3(\rho_p - \rho_f)g - \frac{\pi}{8}C_d\rho_f D^2 u^2 - \frac{\pi}{6}C_a D^3\rho_f\frac{du}{dt} - \frac{3}{2}D^2\sqrt{\pi\rho_f\nu}\int_0^t \frac{du}{d\tau}\frac{d\tau}{(t-\tau)^{1/2}} = \frac{\pi}{6}D^3\rho_p\frac{du}{dt} \qquad (20)$$

The initial condition to Equation (20) is $u(0) = u_0$ where $u_0 \geq 0$. For a dense particle ($\rho_p \gg \rho_f$), the Basset force can be neglected (Ferreira et al., 1998; Jalaal et al., 2010a). Therefore,

$$\frac{\pi}{6}D^3(\rho_p - \rho_f)g - \frac{\pi}{8}C_d\rho_f D^2 u^2 - \frac{\pi}{6}C_a D^3\rho_f\frac{du}{dt} = \frac{\pi}{6}D^3\rho_p\frac{du}{dt} \qquad (21)$$

Putting Equation (9) in (21) and simplifying yields:

$$\frac{du}{dt} + \Omega_1 u + \Omega_2 u^2 - \Omega_3 = 0 \qquad (22)$$

where

$$\Omega_1 = \frac{18(2-\phi)^{1.42229}\nu}{(\sigma + C_a)D^2};$$

$$\Omega_2 = \frac{60.31e^{-6.79646\phi} + 0.33}{(\sigma + C_a)D};$$

$$\Omega_3 = \left(\frac{\sigma - 1}{\sigma + C_a}\right)g.$$

Equation (22) is a Ricatti differential equation and its exact analytical solution has been derived in several studies (Ferreira et al., 1998; Guo, 2011; Big-Alabo et al., 2023; Lain et al., 2023). It can be seen from Equation (22) that the particle experiences a positive deceleration if $\Omega_1 u_0 + \Omega_2 u_0^2 - \Omega_3 < 0$ and a negative deceleration if $\Omega_1 u_0 + \Omega_2 u_0^2 - \Omega_3 > 0$. Applying the exact solutions derived by Big-Alabo et al. (2023), the displacement, velocity, acceleration and settling time of the particle were derived as follows.

Displacement

$$s = \frac{1}{\Omega_2}\left[\ln\left(\frac{\mathcal{K}e^{nt}+1}{\mathcal{K}+1}\right) - (\Omega_2 u_s + \Omega_1)t\right] \quad (23)$$

Velocity

$$u = \frac{1}{2\Omega_2}\left[\frac{n(\mathcal{K}e^{nt}-1)}{\mathcal{K}e^{nt}+1} - \Omega_1\right] \quad (24)$$

Acceleration

$$\frac{du}{dt} = \frac{n^2\mathcal{K}e^{nt}}{\Omega_2(\mathcal{K}e^{nt}+1)^2} \quad (25)$$

Settling time

$$t_s = \frac{1}{n}\ln\left(\frac{(2-\text{sgn}(\Delta u)\,0.01)\Omega_2 u_s + \Omega_1}{\text{sgn}(\Delta u)\,0.01\mathcal{K}\Omega_2 u_s}\right) \quad (26)$$

where sgn is the signum function, $n = 2\Omega_2 u_s + \Omega_1$, $\mathcal{K} = [\Omega_2(u_s + u_0) + \Omega_1]/[\Omega_2(u_s - u_0)]$ and $\Delta u = u_s - u_0$.

Yoghoobi and Torabi (2012) investigated the effect of sphericity on the velocity and acceleration of an initially stationary non-spherical particle falling in a viscous medium. They did not consider the case of non-zero initial velocity or investigate the effect of sphericity on the particle distance. Here we studied the effect of sphericity on the accelerated motion of an initially moving non-spherical particle using Equations (23 – 26). The results for a 3.0 cm glass particle falling in water at an initial velocity of 0.40 m/s are shown in Figures 7 to 9. The properties of glass and water are given in Table 3. The settling distance ranges from 0.0510203 m at $\phi = 0.01$ to 0.51976 m at $\phi = 0.90$ whereas the settling velocity ranges from 0.0913443 m/s at $\phi = 0.01$ to 1.01004 m/s at $\phi = 0.90$. The displacement and velocity were observed to increase with increase in sphericity at all times. However, Figure 8 shows that below a "critical" sphericity the velocity profile decreased from the initial velocity to the settling velocity and above that sphericity the profile increased to the settling velocity. To determine the critical sphericity, the effect of sphericity on the settling time was investigated as shown in Figure 10. At very small sphericities, the drag force is very high and the particle settles very quickly resulting to a settling velocity that is much lower than the initial velocity. As the sphericity increases, the settling velocity increase until it matches the initial velocity. At this point the settling time is zero and the sphericity is equal to the critical sphericity. Figure 10 shows that the critical sphericity (ϕ_c) for the present case study is in the range of 0.458 and 0.465. The actual point could not be predicted in Figure 10 because of the assumption that the actual settling velocity is attained at 99% of the theoretical settling velocity. Using 99.925% of the theoretical settling velocity, the critical sphericity was obtained as $\phi_c \cong 0.4615$, which is the average value of the range, 0.458 to 0.465, for 99.0%. When $\phi > \phi_c$, it means that the drag force has reduced to the point where the settling velocity is higher than the initial velocity. The implication is that $\phi > \phi_c$ results in a positively decelerating particle while $\phi < \phi_c$ results in negatively decelerating particle. When $\phi = \phi_c$, there is no deceleration and the particle experiences a constant velocity motion at the settling velocity.

In Figures 7 to 9, the initial velocity of the particle was greater than zero. For the case of zero initial velocity, the particle only experiences a positive deceleration and the velocity increases from zero to the settling velocity (Yaghoobi and Torabi, 2012). The settling time increases monotonically with sphericity and has no dip in its variation. This is simply explained by the fact that the drag force decreases with increasing sphericity. The reduced drag force causes the initially stationary particle to experience more of the inertia effects, resulting in a higher settling velocity, a longer settling distance and a longer settling time as the sphericity increases.

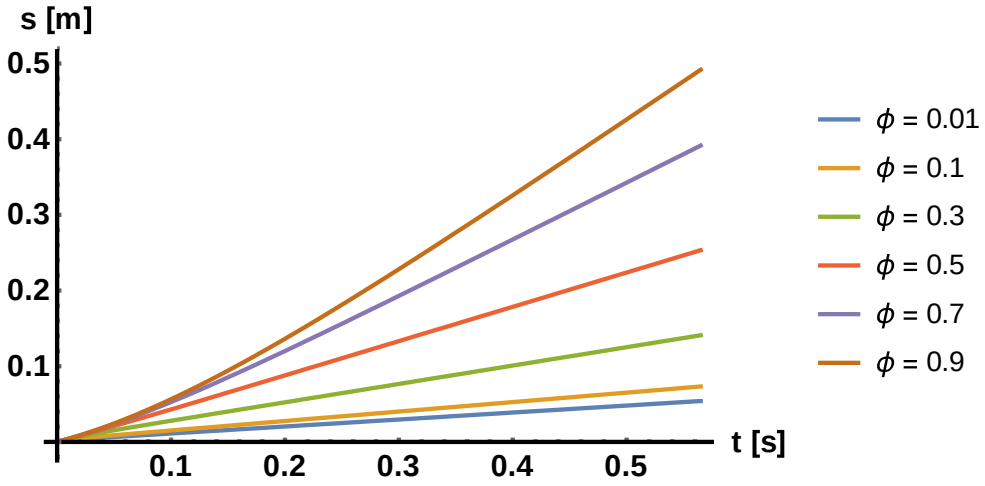

Fig. 7: Effect of sphericity on the displacement of a glass particle falling in water

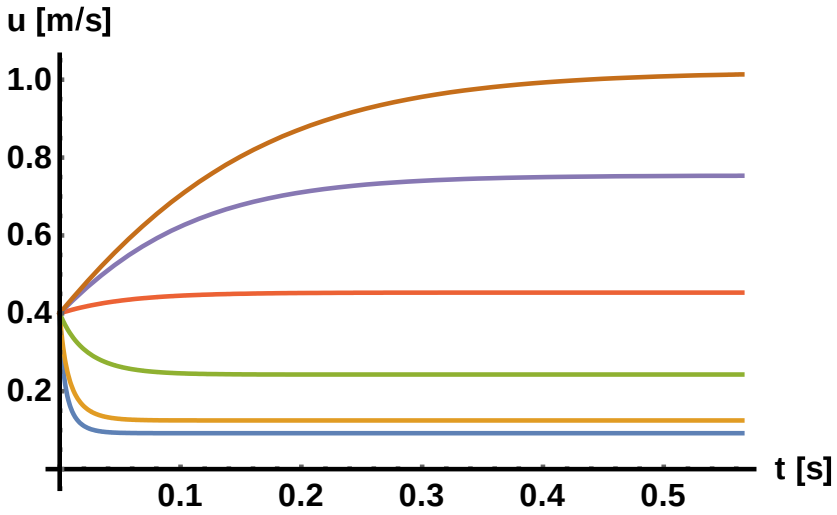

Fig. 8: Effect of sphericity on the velocity of a glass particle falling in water

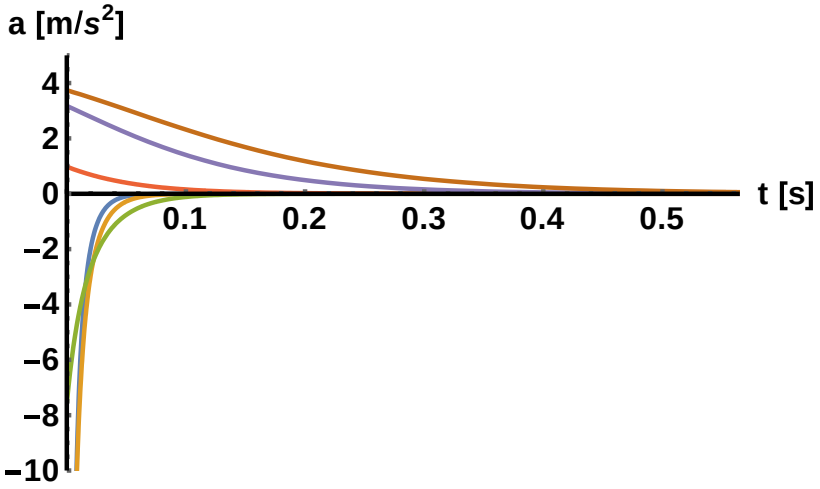

Fig. 9: Effect of sphericity on the acceleration of a glass particle falling in water

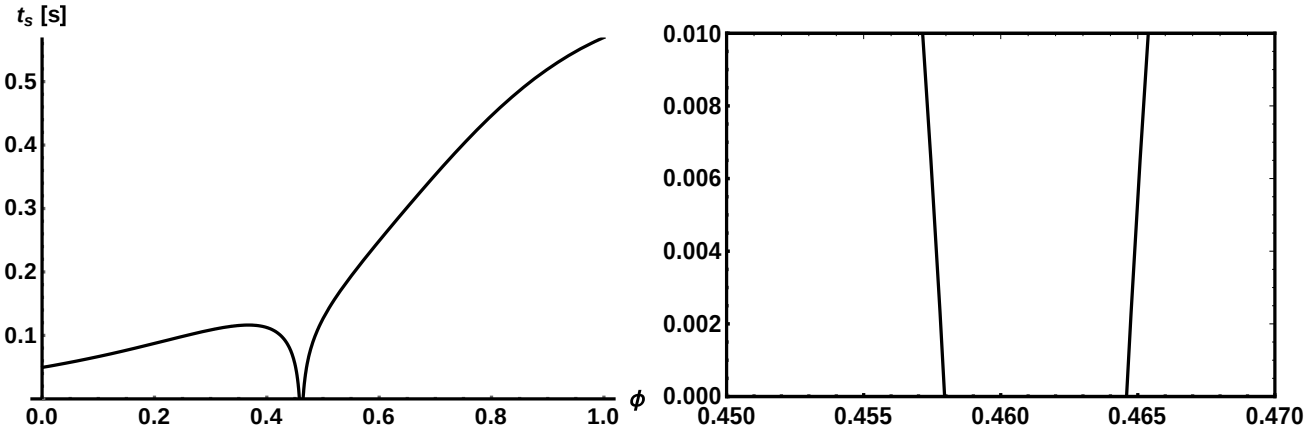

Fig. 10: Effect of sphericity on the settling time of a glass particle falling in water. The right plot is an exploded view of the dip in the left plot.

6. Conclusion

In this study, a new sphericity-dependent drag law was proposed to address identified shortcomings in the drag law of Chien (1994). The new drag law was developed using nonlinear regression analysis and validated using 827 measured data points of $C_d - Re$ relationship for sphericities and Reynolds number in the range of 0.471 – 1.0 and 0.01 – 10000 respectively. An error analysis revealed that the new drag law has an RSME value that is either comparable or significantly better than other sphericity-dependent drag laws with more complicated Reynolds number dependence. An important feature of the new drag law is that it does not introduce additional or complex nonlinearities in the differential equation for a freely falling particle. Hence, the new drag law was applied to derive closed-form solutions for the settling velocity, settling time, fall displacement, fall velocity and fall acceleration. Predictions of the settling velocity solution were shown to compare well with experimental data for non-spherical particles. Simulations of the effect of sphericity on the dynamic response of an initially moving particle showed that the particle can be in positive or negative deceleration depending on the value of the sphericity. Positive deceleration occurs if $\phi > \phi_c$ while the negative deceleration motion occurs when $\phi < \phi_c$, where ϕ_c is the critical sphericity at which there is no deceleration. However, the case of an initially stationary particle only permits positive deceleration and the particle experiences longer settling time, higher settling velocity and longer settling distance as the sphericity increases.

Declaration of conflicting interests

None declared.

Data availability statement

All necessary data for this study has been included in the manuscript.

Funding/acknowledgement

This article is dedicated to honouring Prof Joseph A Ajienka on the occasion of his retirement and 70th birthday.

References

Allen, H.S. (1900). The motion of a sphere in a viscous fluid. Philosophical Magazine 50(306), 519–534.

Bagheri, G., Bonadonna, C. (2016). On the drag of freely falling non-spherical particles. Powder Technology, 301, 526–544.

Big-Alabo, A., Ebieto, C., Ofodu, J. C., Ossia, C. V. (2023). On the gravitational fall of a non-spherical particle in a quiescent fluid medium. Powder Technology, 430, 119017.

Big-Alabo, A., Ezekwem, C. (2021). Accurate solution and analysis of the transient temperature and stability of combustible micron-sized iron particle in gaseous oxidizing environment. International Journal of Applied and Computational Mathematics. 7(3), Article number 57, 18 pages.

Bombardelli, F. A., Chanson, H. (2009). Progress in the observation and modeling of turbulent multi-phase flows. Environmental Fluid Mechanics, 9(2), 121–123.

Chen, H., Ding, W., Wei, H., Saxén, H., Yu, Y. (2022). A Coupled CFD-DEM Study on the

Effect of Basset Force Aimed at the Motion of a Single Bubble. Materials. 15, 5461.

Cheng, N.S. (2009). Comparison of formulas for drag coefficient and settling velocity of spherical particles. Powder Technology, 189(3), 395–398.

Chien, S.-F. (1994). Settling Velocity of Irregularly Shaped Particles. SPE Drilling & Completion, 9(04), 281–289.

Clift, R., Gauvin, W.H. (1971). Motion of entrained particles *in gas streams. Can J Chem Eng. 49, 439–448. https://doi.org/10.1002/cjce.5450490403

Crowe, C., Sommerfeld, M., Tsuji, M. (2011). Multiphase flows with droplets and particles. CRC Press, Boca Raton.

Dioguardi, F., Mele, D., Dellino, P. (2018). A new one-equation model of fluid drag for irregularly shaped particles valid over a wide range of Reynolds number. J Geophys Res Solid Earth. 123, 144–156. https://doi.org/10.1002/2017JB014926.

Ferreira, J.M., Duarte Naia, M., Chhabra, R.P. (1998). An analytical study of the transition motion of a dense rigid sphere in an incompressible Newtonian fluid. Chemical Engineering Communications. 168(1), 45–58.

Ganser, G. H. (1993). A rational approach to drag prediction of spherical and non-spherical particles. Powder Technology. 77, 143–152. https://doi.org/10.1016/0032-5910(93)80051-B

Goossens, W.R.A. (2019). Review of the empirical correlations for the drag coefficient of rigid spheres. Powder Technology, 352, 350–359.

Guo, J.K. (2011). Motion of spheres falling through fluids. Journal of Hydraulic Research, 49(1), 32–41.

Haider, A., Levenspiel, O. (1989). Drag coefficient and terminal velocity of spherical and nonspherical particles. Powder Technology, 58(1), 63–70.

Hazzab, A., Terfous, A., Ghenaim, A. (2008). Measurement and modeling of the settling velocity of isometric particles. Powder Technology, 184(1), 105–113.

Jalaal, M., Ganji, D.D., Ahmadi, G. (2010a). Analytical investigation on acceleration motion of a vertically falling spherical particle in incompressible Newtonian media. Advanced Powder Technology. 21(3), 298–304.

Jalaal, M., Ganji, D.D., Ahmadi, G. (2010b). An analytical study on settling of non-spherical particles. Asia-Pacific Journal of Chemical Engineering, 7(1), 63–72.

Julien, P.Y. (2010). Erosion and sedimentation 2nd ed. Cambridge University Press, Cambridge MA.

Krafcik, A., Babinec, P., Frollo, I. (2018). Stokes versus Basset: comparison of forces governing motion of small bodies with high acceleration. European Journal of Physics, 39(3), 035805.

Laín, S., García, D.F., Gandini, M.A. (2023). Analytical Solutions of the Riccati Differential Equation: Particle Deposition in a Viscous Stagnant Fluid. Mathematics, 11, 3262. doi:10.3390/math11153262.

Lapple, C.E., Shepherd, C.B. (1940). Calculation of particle trajectories. Ind. Eng. Chem. 32(4), 605–617.

Li, T., Li, S., Zhao, J., Lu, P., Meng, L. (2012). Sphericities of non-spherical objects. Particuology, 10(1), 97–104.

Liu, X., Wang, J., Chai, Z., Min, F., Jiang, X., Zhu, K., Dai, J. (2022). New model for predicting terminal settling velocity and drag coefficient of the Oncomelania. Front Environ Sci. 10, 1051392. doi:10.3389/fenvs.2022.1051392.

Loth, E. (2008). Drag of non-spherical solid particles of regular and irregular shape. Powder Technol. 182, 342–353. https://doi.org/10.1016/j.powtec.2007.06.001.

Maggi, F. (2013). The settling velocity of mineral, biomineral, and biological particles and aggregates in water, J. Geophys. Res. Oceans, 118, 2118–2132.

Michaelides, E.E, Feng, Z. (2023). Review – Drag coefficients of non-spherical and irregularly shaped particles. Journal of Fluids Engineering, 145(060801), 1–20.

Moorman, R.W. (1955). Motion of a spherical particle in the acceleration portion of free fall. Ph.D. dissertation. University of Iowa, Iowa City IA.

Terfous, A., Hazzab, A., Ghenaim, A. (2013). Predicting the drag coefficient and settling velocity of spherical particles. Powder Technology. 239, 12–20.

Torabi, M., Yaghoobi, H. (2012). Accurate solution for acceleration motion of a vertically falling spherical particle in incompressible Newtonian media. The Canadian Journal of Chemical Engineering, 91(2), 376–381. doi:10.1002/cjce.21641.

Wadell, H. (1934). The coefficient of resistance as a function of Reynolds number for solids of various shapes, J. Franklin Inst., 217, 459-490.

Yaghoobi, H., Torabi, M. (2012). Analytical solution for settling of non-spherical particles in incompressible Newtonian media. Powder Technology, 221, 453–463.

Yang, F., Zeng, Y-H., Huai, W-X. (2021). A new model for settling velocity of non-spherical particles. Environmental Science and Pollution Research. https://doi.org/10.1007/s11356-021-14880-9.

Yin, Z., Wang, Z., Liang, B. and Zhang, L. (2017). Initial Velocity Effect on Acceleration Fall of a Spherical Particle through Still Fluid. Mathematical Problems in Engineering. 2017, Article ID: 9795286, 8 pages.

Yow, H. N., Pitt, M. J., Salman, A. D. (2005). Drag correlations for particles of regular shape. Advanced Powder Technology, 16(4), 363–372.

Zolfagharian, A., Darzi, M., Ghasemi, S.E. (2017). Analysis of nano droplet dynamics with various sphericities using efficient computational techniques. J. Cent. South Univ. 24, 2353−2359.